Dirac-equation description of the electronic states of graphene with a line defect: Wave-function connection condition

Jiang Liwei, Yu Guodong, Gao Wenzhu, Liu Zhe, and Zheng Yisong

Dirac-equation description on the electronic states of graphene in the presence of a line defect: wavefunction connection condition

Jiang Liwei, Yu Guodong, Gao Wenzhu, Liu Zhe, and Zheng Yisong[*]

National Laboratory of Superhard Materials, Department of Physics, Jilin University, Changchun 130012, China

(Dated: September 14, 2012)

The presence of an extended line defect in graphene brings about some interesting electronic properties to such a truly two-dimensional (2D) carbon material, such as the energy band engineering and valley filtering. By establishing an appropriate connection condition for the spinor wavefunction across the line defect, we find that the massless Dirac equation is still a valid theoretical model to describe low-energy electronic properties of the line defect embedded graphene structure. To check the validity of the wavefunction connection condition, we take two kinds of line defect embedded graphene structures as examples to study the low-energy electronic states by solving the Dirac equation. Firstly, for a line defect embedded zigzag-edged graphene nanoribbon, we obtain analytical results about the subband dispersion and eigen wavefunction, which coincide well with the numerical results from the tight-binding approach. Then, for a 2D graphene embedded with an extended line defect, we get an exact expression about the valley polarized electronic transmission probability, which demonstrates the simple result estimated previously in zero-energy limit. More interestingly, our analytical result indicates that in such a 2D graphene structure a quasi one-dimensional (1D) electronic state occurs along the line defect. And the electronic group velocity in this quasi 1D electronic state can be readily modulated by applying a strain field around the line defect.

I. INTRODUCTION

Because of the presence of dislocations, microcracks, grain boundaries, phase interfaces, etc. in their growth,[1–10] experimentally obtained graphene samples are not always single-crystalline materials. The aligned adjoining grains make grain boundaries intrinsic topological defects[11] which are expected to markedly alter the electronic properties in graphene without the need to introduce exotic atoms.[12,13] Recently, an extended line defect of millimeter scale in an epitaxial layer of graphene was successfully fabricated.[10,14] Subsequently, it was demonstrated that during the growth of graphene by chemical vapor deposition, the crystallographic orientation and the size of individual grains can be controlled.[15] These experimental results indicate that graphene in the presence of line defects is currently a practical structure, which certainly merits further investigations, both experimentally and theoretically.

Although there are many kinds of extended line defects in graphene,[16] in the present work we will only focus on one kind of them, which is composed of a periodic repetition of one octagon plus two pentagons, see Fig. 1. Some recent theoretical investigations revealed many interesting electronic properties when such a line defect emerges in graphene. At first, such a line defect can be utilized as a valley filter because the transmission probability of a low-energy electron incident upon it shows notable valley polarization.[17] Secondly, around the line defect the electronic spin polarization also occurs, though it is much weaker than the valley polarization.[18] Thirdly, when the line defect is embedded in a zigzag-edged graphene nanoribbon, it introduces new conductance quantization values and modifies the conductance quantization threshold.[19] Furthermore, when the line defect is positioned very close to one of the zigzag edge, the graphene nanoribbon shows a half-metallic subband structure.[20]

To our knowledge, most theoretical investigations, e.g., the aforementioned works, on the electronic properties of graphene in the presence of line defects are so far based on the tight-binding (TB) model or the ab-*initio* calculations. It is well known that within a continuum model the low-energy (in the vicinity of Fermi level) electronic properties of graphene can be well described by a massless 2D Dirac equation .[21–23] In such a theoretical framework, it is usually possible to get analytical results about the electronic eigen states.[24,25] And thereby many electronic properties unique to graphene can be understood intuitively,[26] such as the chiral tunneling[27] and the integer quantum Hall effect.[24,28] Additionally, as for graphene nanoribbons,[29] graphene with a reconstructed zigzag edge,[30] and graphene with a terminated honeycomb lattice along an arbitrary direction,[31] the low-energy electronic properties of these structures can be well treated within such a continuum model, provided that the Dirac equation is supplemented by appropriate boundary conditions. Motivated by these theoretical advances, we attempt to generalize the Dirac-equation approach to the line defect embedded graphene structures. In view of the nontrivial role of the line defect in modulating the low-energy electronic properties of graphene, such a theoretical method is highly desirable.

In this work, we will show that the low-energy electronic states of graphene in the presence of an extended line defect can be described by Dirac equation if it is supplemented by an appropriate wavefunction connection condition across the line defect. With the help of TB model, we establish such a connection condition obeyed by the spinor wavefunction in the Dirac equation. Then, in order to demonstrate the validity of the obtained connection condition, we derive the eigen solutions of the Dirac equation of a zigzag-edged graphene nanoribbon with an extended line defect parallel to the ribbon edges (hereafter this structure is abbreviated to LD-ZGNR). We find that the obtained subband structures agree well with the TB results. In addition, taking a line defect embedded 2D bulk graphene structure (we denote this structure as LD-BG) as an example, by means of such a connection condition, we obtain an exact expression of the valley polarized transmission probability when an electron passes through the line defect. This result proves the simple result estimated previously in zero-energy limit.[17] More importantly, our analytical result indicates that in such an LD-BG a quasi 1D electronic state exists around the line defect. And the electronic group velocity in such a state can be readily tuned by applying a strain field along the extended line defect. Accordingly, the extended line defect can be viewed as a 1D quantum wire to carry the current in an LD-BG sample.

The rest of this paper is organized as follows: In section II, a detailed derivation of the spinor wavefunction connection condition across the line defect in graphene is presented. Then in section III the electronic eigen states of A): an LD-ZGNR and B): an LD-BG are, respectively, obtained by solving the Dirac equation subject to the wavefunction connection condition. Finally, the main results are summarized in section IV.

II. THE WAVEFUNCTION CONNECTION CONDITION FOR DIRAC EQUATION

The lattice structure of a line defect embedded graphene is illustrated in Fig. 1. The topological geometry of the line defect consists of the periodic repetition of one octagonal plus two pentagonal rings along y direction.[10] For conduction electrons in this structure, the TB Hamiltonian within the nearest-neighbor approximation can be formally written as

$$H_{TB} = \sum_{<nj,n'j'>} t_{nj,n'j'} |nj\rangle\langle n'j'| \tag{1}$$

with $|nj\rangle$ standing for the Wannier state localized at the jth atom of the nth layer. As seen in Fig. 1, an individual carbon atom at a lattice point can be specified by a pair of indexes (n, j). The notation $\langle nj, n'j'\rangle$ means that the summation is restricted within the nearest-neighbor atomic pairs. In the bulk region, the hopping energy $t_{nj,n'j'}$ takes a uniform value $t_{nj,n'j'} = t = -3$eV. On the other hand, associated with the line defect, we define two hopping energies (τ_1 and τ_2) to account for the possible lattice distortion. Within the TB model, the Schrödinger equation can be written in a form as

$$[E - H_{TB}(n, n)]\psi_{TB}(n) = H_{TB}(n, n-1)\psi_{TB}(n-1) + H_{TB}(n, n+1)\psi_{TB}(n+1), \tag{2}$$

where $H_{TB}(n, n')$ is the TB Hamiltonian matrix which describes the interaction between the nth and n'th layer. The wavefunction $\psi_{TB}(n) = [\cdots, \psi_{TB}(n, -1), \psi_{TB}(n, 0), \psi_{TB}(n, 1), \cdots]^T$ with $\psi_{TB}(n, j)$ being the electronic probability amplitude at a lattice point (n, j). Hereafter we adopt the shorthands $\overline{j} = -j$ and $\overline{n} = -n$ for convenience. We take the line defect as the $n = 0$ layer (as shown in Fig. 1). Just following Eq. (2), we write out the concrete TB equations centered at $n = \overline{1}, 0, 1$ layers below, since they will be employed in our sequent formulation. They are given by

$$\begin{cases} E\psi_{TB}(\overline{1}) = \tau_1\psi_{TB}(0) + U\psi_{TB}(\overline{2}) \\ (E - \Sigma)\psi_{TB}(0) = \tau_1\psi_{TB}(1) + \tau_1\psi_{TB}(\overline{1}) \\ E\psi_{TB}(1) = \tau_1\psi_{TB}(0) + U\psi_{TB}(2) \end{cases}, \tag{3}$$

where U, the atomic interaction between the adjacent layers, is an infinite matrix with its element defined as $[U]_{jj'} = t(\delta_{j,j'} + \delta_{j,j'-1})$ ($\delta_{j,j'}$ is the Kronecker delta function); And $\Sigma = \tau_2 \text{Diag}[\cdots, \sigma, \sigma, \sigma, \cdots]$ with σ being x component of Pauli matrix, standing for the interaction of the atoms in the line defect. It can be readily seen from Fig. 1 that $\psi_{TB}(\overline{1})$ and $\psi_{TB}(1)$ just correspond to atoms of two distinct sublattices (A and B respectively).

Since we are only concerned with the low-energy electronic states, it seems suitable to adopt the $\boldsymbol{k} \cdot \boldsymbol{p}$ approximation,[25,32] which is characterized by a massless 2D Dirac equation for graphene. First of all, we need to establish a coordinate frame for such a continuum model, which is illustrated in Fig. 1. In the bulk region far from the line defect, there is no problem that the low-energy electronic state can be solved through Dirac equation

$H_D \Psi_D = E \Psi_D$. The Dirac Hamiltonian is given by

$$H_D = \gamma \begin{bmatrix} 0 & \hat{k}_- & 0 & 0 \\ \hat{k}_+ & 0 & 0 & 0 \\ 0 & 0 & 0 & \hat{k}_- \\ 0 & 0 & \hat{k}_+ & 0 \end{bmatrix}, \tag{4}$$

and the spinor wavefunction has the form

$$\Psi_D = \left[u_D^A, -\mathrm{i} u_D^B, \mathrm{i}\tilde{u}_D^B, -\tilde{u}_D^A \right]. \tag{5}$$

In the above equations, $\gamma = \sqrt{3}at/2$ with a being the lattice constant of pristine graphene. $\hat{k}_\pm = \hat{k}_x \pm \mathrm{i}\hat{k}_y$ and $\hat{k}_{x(y)} = -\mathrm{i}\partial_{x(y)}$ is an operator to measure the momentum deviation from the Dirac point $\mathbf{K} = (0, -4\pi/3a)$ or $\mathbf{K}' = (0, 4\pi/3a)$. In the spinor wavefunction Ψ_D, the components u_D^X and $\tilde{u}_D^X$ stand actually for the envelope function of $X \in \{A, B\}$ sublattice points in $\mathbf{K}$ and $\mathbf{K}'$ valleys respectively. Because that the TB model and Dirac equation are both involved in our formulation, as we have done, we adopt subscripts TB and D (Dirac equation) to the respective Hamiltonians and wavefunctions to avoid confusion.

In the vicinity of a line defect, the eigen wavefunction becomes more complicated. Strictly speaking, even for an eigen state with a very low eigen energy, the electronic probability amplitudes on the atoms quite close to the line defect can not be completely determined by a solution of the Dirac equation. We now explain such a viewpoint in detail based on an argument presented in Ref. [30]. Suppose that there are two Bloch states with a wavevector component difference $q_y - q_y' = -\pi/a$, where $q_y = K_y(K_y') + k_y$ is the y component of the electronic wavevector measured from the Brillouin zone center. For a pristine graphene, they are certainly two independent electronic eigen states. However, the presence of an extended line defect makes the translational period in y direction twice, i.e., it is equal to $2a$, rather than a. As a result, the above two Bloch states correspond to the same point in the reduced Brillouin zone of the line defect embedded graphene. Therefore, an eigen state of graphene in the presence of a line defect is a linear combination of such two Bloch states. Now we consider a very low-energy eigen state who consists of two Bloch states. Suppose that one component Bloch state of this eigen state possesses a wavevector component q_y which is in the vicinity of $\mathbf{K}$ valley of a pristine graphene. Thus the slow-varying part of such a component of the eigen state obeys the Dirac equation. Meanwhile, the other Bloch state in the eigen state has a wavevector component q_y' in the vicinity of $(0, -\pi/3a)$. In a pristine graphene, such a Bloch state corresponds to a relatively high eigen energy since it is far from the Dirac points. However, when a line defect is embedded in graphene, such a Bloch state has its contribution to the eigen state, but it is supposed to possess an imaginary wavevector component along x direction since the eigen energy has been assumed to be very small. In addition, because that the Brillouin zone folding caused by the doubling of translational period in y direction does not mix the $\mathbf{K}$ and $\mathbf{K}'$ valleys, we can treat the eigen states in the two valleys separately. To sum up the above analyses, for an eigen state in the $\mathbf{K}$ valley, we can denote it as

$$\psi_{TB}(x,y) = u_D^X(x,y)e^{-\mathrm{i}y4\pi/3a} + \phi_{loc}^X(x,y)e^{-\mathrm{i}y\pi/3a}, \tag{6}$$

where the propagating mode $u_D^X(x,y)$ obeys the Dirac equation, and the localized mode $\phi_{loc}^X(x,y)$ decays rapidly as going away from the line defect. Below we will see that such a classification is reasonable. In the above expression, although we have explicitly written out y dependence of the envelope functions $u_D^X(x,y)$ and $\phi_{loc}^X(x,y)$, it should be emphasized that these functions are slow-varying ones along this orientation in the scale of graphene lattice constant. If we employ such an expression only in a local region, say, around a lattice point (n, j), it can be approximatively changed into a form as

$$\psi_{TB}(n,j) = u_D^X(n)e^{-\mathrm{i}4\pi j(n)/3} + \phi_{loc}^X(n)e^{-\mathrm{i}\pi j(n)/3}, \tag{7}$$

with

$$\begin{cases} j(n) = j, & \text{for} \quad n = \pm 1, \pm 4, \pm 5, \pm 8 \cdots, \\ j(n) = j + 1/2, & \text{for} \quad n = \pm 2, \pm 3, \pm 6, \pm 7 \cdots. \end{cases} \tag{8}$$

Note that the sublattice attribution of the wavefunction $\psi_{TB}(n,j)$ is determined by the layer index n. When the condition of low-energy limit $E \to 0$ is used, from the TB equation we can get the following relations of the envelope functions. For neighboring layers in the right-hand side of the line defect, we have

$$u_D^A(n+3) = u_D^A(n+1), \quad u_D^B(n+2) = u_D^B(n),$$

$$\phi_{loc}^A(n+3) = \frac{1}{\sqrt{3}}\phi_{loc}^A(n+1), \quad \phi_{loc}^B(n) = 0, \tag{9}$$

with $n = 1, 3, 5, \cdots$. On the other hand, in the close region to the left of the line defect, the same relations hold true except that a swap of the sublattice attribution to these functions should be made. This result indicates that $u_D^X(x, y)$'s are slow-varying envelope functions which just follow the Dirac equation, whereas $\phi_{loc}^X(x, y)$'s only exist in the vicinity of the line defect. And they can not be described by the Dirac equation. It should be noted that a similar result was previously derived to determine the boundary condition at the lattice edge of graphene.[31]

Under the condition $E \to 0$, and after eliminating the term $\psi_{TB}(0)$, the TB equation (3) then evolves into

$$
\begin{cases}
\mathcal{F}\psi_{TB}(1, j) = -\mathcal{F}\psi_{TB}(\overline{1}, j) + \psi_{TB}(\overline{2}, j-1) + \psi_{TB}(\overline{2}, j-2) \\
\mathcal{F}\psi_{TB}(1, j-1) = -\mathcal{F}\psi_{TB}(\overline{1}, j-1) + \psi_{TB}(\overline{2}, j) + \psi_{TB}(\overline{2}, j-1) \\
\mathcal{F}\psi_{TB}(\overline{1}, j) = -\mathcal{F}\psi_{TB}(1, j) + \psi_{TB}(2, j-1) + \psi_{TB}(2, j-2) \\
\mathcal{F}\psi_{TB}(\overline{1}, j-1) = -\mathcal{F}\psi_{TB}(1, j-1) + \psi_{TB}(2, j) + \psi_{TB}(2, j-1)
\end{cases}
, \tag{10}
$$

with $\mathcal{F} = \tau_1^2/t\tau_2$ and $j = \cdots, \overline{3}, \overline{1}, 1, 3, \cdots$. Substituting Eqs. (7-9) into Eq. (10) and eliminating the localized modes, we finally obtain the connection condition of the spinor wavefunction in Dirac equation. It is given by

$$
\begin{aligned}
u_D^B(0^-) &= u_D^A(0^+) \\
\mathcal{F}u_D^A(0^-) - u_D^B(0^-) &= u_D^A(0^+) - \mathcal{F}u_D^B(0^+).
\end{aligned} \tag{11}
$$

$u_D^X(0^\pm)$ represents the envelope function very close to the left (0^-) or the right (0^+) of the line defect. By the same token, we can obtain the connection condition in $\mathbf{K}'$ valley. As a result, we find that $\tilde{u}_D^X(0^\pm)$ obeys the same equation as given above for $u_D^X(0^\pm)$. Eq. (11) is our central result, by which the Dirac equation can be used to quantitatively describe the low-energy electronic states when a line defect is present in a graphene structure.

III. ELECTRONIC EIGEN STATES OF DIRAC EQUATION

In order to confirm the validity of the wavefunction connection condition we have developed, we choose two representative graphene structures to solve the eigen states of Dirac equation. The first one is an LD-ZGNR whose electronic and transport properties have been previously calculated by a TB model.[19] It has been reported that the line defect behaves as an effective third edge and can be used as a quantum wire.[19] The second one is an LD-BG, in which the line defect has been reported to give rise to the valley filtering effect.[17] To comparing the dispersion relation and the wavefunction obtained by solving the Dirac equation with the TB numerical result, we find both results agree with each other very well in low-energy region. This indicate unambiguously the validity of the connection condition we have developed.

Although our main objective to treat theoretically the two line defect embedded graphene structures is to check the applicability of the wavefunction connection condition, some interesting results obtained from the Dirac-equation approach are noteworthy. First, for the LD-ZGNR, we obtain the analytical wavefunction of an electronic eigen state, which is useful to study the electronic transport or optical properties of such a structure. Then, for the LD-BG, we find a kind of quasi 1D eigen state along the line defect, thus the line defect acts as a quantum wire to carry current along a specific direction in a 2D graphene sheet. Besides, we get an exact expression about the valley polarized electronic transmission probability through the line defect. This result is energy independent, which demonstrates the simple result estimated previously in zero-energy limit. Next we will present these results in detail.

A. Zigzag-edged graphene nanoribbon with a line defect

We now consider an LD-ZGNR with the extended line defect parallel to the ribbon edges. The width of the nanoribbon with a line defect is denoted as $W = L_1 + L_2$, where L_1 and L_2 are the widths from the left and right edges of the nanoribbon to the line defect respectively. Without loss of generality, in this subsection we only consider the case of $\tau_1 = \tau_2 = t$, namely, $\mathcal{F} = 1$ for simplicity. Besides the connection condition shown in Eq. (11), the wavefunction is subject to the following boundary conditions at the zigzag edges of the nanoribbon:

$$
u_D^A(x = -L_1, y) = u_D^B(x = L_2, y) = 0. \tag{12}
$$

To satisfy these conditions, an allowed eigen wavefunction of the Dirac equation in $\mathbf{K}$ valley takes a form as

$$\Psi_D^K = \begin{bmatrix} u_D^A \\ -iu_D^B \end{bmatrix} = \begin{cases} ze^{ik_y y}\begin{bmatrix} \varepsilon \sin k_x(x+L_1) \\ i\left[k_y \sin k_x(x+L_1) - k_x \cos k_x(x+L_1)\right] \end{bmatrix}, -L_1 \le x \le 0 \\[2em] ze^{ik_y y}\begin{bmatrix} \left[k_y \sin k_x(x-L_2) + k_x \cos k_x(x-L_2)\right] \\ i\varepsilon \sin k_x(x-L_2) \end{bmatrix}, 0 \le x \le L_2 \end{cases}$$

(13)

where the normalized constant is

$$z = \lambda\varepsilon\Big\{\varepsilon^2(k_y \sin k_x L_1 - k_x \cos k_x L_1)^2 \cdot$$

$$\left[\varepsilon^2 L_2 - k_y/k_x \sin k_x L_2(k_y \cos k_x L_2 + k_x \sin k_x L_2)\right] + L_1 \rightleftharpoons L_2\Big\}^{-1/2}$$

(14)

with $\lambda = (k_x \cos k_x L_2 - k_y \sin k_x L_2)$ for $-L_1 \le x \le 0$ and $\lambda = (k_x \cos k_x L_1 - k_y \sin k_x L_1)$ for $0 \le x \le L_2$. The notation $L_1 \rightleftharpoons L_2$ means a term produced by exchanging L_1 and L_2 in the former term. The corresponding eigen energy E satisfies the following transcendental equation

$$(\varepsilon k_y + k_y^2 - k_x^2) + k_x(\varepsilon + 2k_y)\tan k_x(L_1 + L_2) = \varepsilon(\varepsilon + k_y)\frac{\cos k_x(L_1 - L_2)}{\cos k_x(L_1 + L_2)}$$

(15)

with

$$\varepsilon = \frac{E}{\gamma} = \eta\sqrt{k_x^2 + k_y^2},$$

(16)

where $\eta = 1$ or -1, corresponds to the conduction or valence band respectively. Due to the property of translational invariance in y direction, only real k_y is allowed. In contrast, the electronic wavevector component k_x can take an imaginary value. In such a case, by making a simple substitution $k_x = i\alpha$ with $\alpha > 0$, we can see from Eq. (13) that the electronic wavefunction decays exponentially as it goes away from the zigzag edges or the line defect. We call such a kind of eigen state as the edge state. On the other hand, for a real k_x the above solution is referred to as the confined state. In addition, as seen from Eq. (13), the nature of standing wave of the eigen wavefunction in x direction indicates that $+k_x$ and $-k_x$ correspond to the same eigen state. Thereby we need only consider the case of $k_x \ge 0$.

In Fig. 2 we compare low-energy subband structures in $\mathbf{K}$ valley of LD-ZGNRs calculated by the Dirac-equation and the TB approaches respectively. For all calculated results shown in this figure, the characteristic width L_1 of an LD-ZGNR is fixed at a large value, i.e., $L_1 = 75\sqrt{3}a \approx 32$nm. Figs. 2(a) and (b) show the case of $L_2 = 25\sqrt{3}a \approx 11$nm. We can find that the calculated results of the two approaches agree well with each other in the wavevector range $-0.3/2a \le k_y \le 0.4/2a$. This implies that the Dirac equation plus the wavefunction connection condition can quantitatively describe the electronic states in the energy range of ± 450meV around the Fermi level, even though L_2, the smaller characteristic width of the LD-ZGNR, is as small as 10nm. We wonder whether the Dirac-equation approach still works well if L_2 gets smaller. A result with $L_2 = 5\sqrt{3}a \approx 2$nm is shown in Figs. 2(c) and (d). We can see that the coincidence between the results of Dirac-equation and TB approaches becomes poor even if k_y is close to the Dirac point. More precisely, the Dirac equation works well in the wavevector range $-0.3/2a \le k_y \le 0.13/2a$. However, when $k_y > 0.13/2a$ the dispersion calculated by Dirac equation shows an appreciable deviation from the TB result, even if it is still in the relatively low-energy range. This result can be readily understood by calculating the electronic probability distributions (the squared wavefunctions) of an eigen state on the lattice points in a unit cell of the LD-ZGNR.

In Fig. 3 we select some representative eigen states (labeled in Figs. 2(c) and (d)) to show their electronic probability distributions on the lattice points in a unit cell. Figs. 3(a) and (b) show the results for the two eigen states which are labeled by points 1 and 2 at $k_y = 0.014/2a$ in Fig. 2(d) respectively. For these states the eigen energies obtained by Dirac equation are not too bad, see Fig. 2(d). In contrast, Fig. 3(c) depicts the result of an eigen state labeled by point 3 in Fig. 2(c) at $k_y = 0.344/2a$, for which the eigen energy obtained by the Dirac equation becomes poor. From the results shown in Fig. 3 we infer that those eigen states to which the Dirac equation is valid are largely localized in the left side (the wider side) of the line defect. On contrary, some eigen states are almost localized in the right (narrower) side of the line defect, to which the Dirac-equation description is invalid. In other words, the line defect acts as a third edge to divide the nanoribbon into two smaller ones. And both of them contribute to the subbands of the LD-ZGNR. When the smaller characteristic width L_2 becomes too small, only part of the subbands

which just correspond to the eigen states localized in the narrower side of the line defect can not be quantitatively described by Dirac-equation approach. In addition, from the results shown in Fig. 3 we can see that the analytical spinor wavefunction can correctly describe the electronic probability distribution on the lattice points by comparing with the TB results, except the range very close to the line defect. It is the localized mode emerging in Eq. (6) to make the Dirac equation unable to give an accurate result of the electronic probability distribution on the lattice points in the vicinity of the line defect.

B. Infinite graphene with a line defect

Now we turn to treat the electronic states in an LD-BG with an extended line defect at $x = 0$. Due to the mirror symmetry of the lattice with respect to the line defect, an eigen state of the LD-BG obtained from Dirac equation has the conserved odd or even parity. For the odd-parity eigen wavefunction, the connection condition reduces to $u_D^A(0^+) = u_D^B(0^-) = 0$. So that the odd-parity solution is equivalent to the eigen state of two identical semi-infinite graphenes. The electronic states of the semi-infinite graphene were detailedly studied with the Dirac equation in previous literatures.[24,25] Therefore, herein we need only to deal with the even-parity eigen solution. By means of the symmetry $\psi_{TB}(n) = \psi_{TB}(\overline{n})$ we can reduce the connection condition to

$$u_D^A(0^+) = \mathcal{F} u_D^B(0^+). \tag{17}$$

In the same way one can derive the connection condition of $\mathbf{K}'$ valley which has the same form.

In principle, with the help of the connection condition (17), all the even-parity eigen states can be worked out from Dirac equation. For the extended eigen states, the electronic wavevector components k_x and k_y are independent, thus the dispersion relation just follows the one of the pristine graphene, namely, $E = \eta\gamma\sqrt{k_x^2 + k_y^2}$. However, from the eigen solutions of the Dirac equation subject to the connection condition (17) we can obtain a quasi 1D eigen state unique to the LD-BG structure. By letting $k_x = i\alpha$ with $\alpha > 0$, such an interesting eigen wavefunction in $\mathbf{K}$ valley takes an explicit form as

$$\Psi_D^K = \begin{bmatrix} u_D^A \\ -iu_D^B \end{bmatrix} = \begin{cases} \sqrt{\alpha/[2k_y(\alpha + k_y)]}e^{\alpha x}\begin{bmatrix} i(\alpha + k_y) \\ -\varepsilon \end{bmatrix}, x \le 0 \\ \sqrt{\alpha/[2k_y(\alpha + k_y)]}e^{-\alpha x}\begin{bmatrix} -i\varepsilon \\ \alpha + k_y \end{bmatrix}, x \ge 0 \end{cases} \tag{18}$$

with

$$\alpha = -(\varepsilon\mathcal{F}^{-1} + k_y). \tag{19}$$

And the corresponding eigen energy is given by

$$\varepsilon = -2k_y/(\mathcal{F} + \mathcal{F}^{-1}). \tag{20}$$

Note that the condition $\alpha > 0$ requires $\mathcal{F} < 1$. This implies that the lattice distortion is needed for the appearance of such a quasi 1D state. From the above expressions, we can find that the quasi 1D state is localized around the line defect. The localization strength and the electronic group velocity are associated with the parameter $\mathcal{F}$. This indicates that this eigen state can be tuned by applying a strain field around the line defect. As a result, the line defect can be viewed as a 1D quantum wire to carry the current in a bulk graphene sample. Besides, when the eigen energy is very small, in such a quasi 1D state the electron mainly distributes on A sublattice if $x \le 0$ whereas on B sublattice if $x \ge 0$. We choose $\tau_1 = 0.5t$ and $\tau_2 = 1.0t$, hence $\mathcal{F} = 0.25 < 1$, to calculate the edge state dispersion relation from Eq. (20). The result is shown in Fig. 4. Meanwhile, a comparison with the corresponding TB result is made (The TB result is calculated by means of an LD-ZGNR of a width $L = 500\sqrt{3}a$ subject to a periodic boundary condition). We find that the dispersion of this quasi 1D state deviates from the Dirac cone of the bulk band. And the calculated results of the two approaches agree with each other very well when the electronic wavevector does not go too far from the Dirac point. From Fig. 4 we can readily find that due to the presence of this quasi 1D state, the electron-hole symmetry in the dispersion of the LD-BG no longer holds true. In fact, this is a direct result of the breaking of sublattice (chiral) symmetry caused by the line defect. To observe the subband structures shown in Fig. 2, we can see that the electron-hole symmetry is also destroyed by the line defect in LD-ZGNRs. The same result can also appear in a reconstructed zigzag-edged graphene nanoribbon because the edge reconstruction causes the breaking of sublattice (chiral) symmetry.[30]

Next we discuss the valley filtering effect in the LD-BG which was firstly pointed out in Ref. [17]. Therein a simple expression of the electronic transmission probability for an electron to pass through the line defect showed a notable valley polarization, regardless of the energy of the incident electron. But such a result was obtained in zero-energy limit. Therefore, it remains a problem whether and how the valley polarization effect is influenced by a nonzero incident electron energy. By means of the wavefunction connection condition we have just established, it is possible to derive an exact expression about the electronic transmission probability through the line defect as a function of the incident electron energy. In so doing, we need only to consider the scattering of a $\mathbf{K}$ valley electron by the line defect (the case of $\mathbf{K}'$ valley can be treated alike). For a Dirac electron with an energy $\varepsilon = \eta\sqrt{k_x^2 + k_y^2} = \eta k$ ($k_x > 0$), the wavefunction at the left of the line defect consists of an incident and a reflected wave, which can be denoted as

$$[\Psi_D^K]_{left} = \begin{bmatrix} u_D^A \\ -\mathrm{i}u_D^B \end{bmatrix} = \begin{bmatrix} \mathrm{i} \\ \mathrm{i}k_x - k_y \end{bmatrix} \cdot \frac{1}{\sqrt{2}} e^{\mathrm{i}k_y y + \mathrm{i}k_x x} + r_K \begin{bmatrix} \mathrm{i} \\ -\mathrm{i}k_x - k_y \end{bmatrix} \cdot \frac{1}{\sqrt{2}} e^{\mathrm{i}k_y y - \mathrm{i}k_x x}, \tag{21}$$

while the wavefunction at the right of the line defect describes the electronic transmission through the line defect. It then takes a form as

$$[\Psi_D^K]_{right} = \begin{bmatrix} u_D^A \\ -\mathrm{i}u_D^B \end{bmatrix} = t_K \begin{bmatrix} \mathrm{i} \\ \mathrm{i}k_x - k_y \end{bmatrix} \cdot \frac{1}{\sqrt{2}} e^{\mathrm{i}k_y y + \mathrm{i}k_x x}. \tag{22}$$

In the above equations, r_K and t_K denote the reflection and transmission probability amplitudes respectively. By means of the wavefunction connection condition we can establish a relation between the spinor wavefunctions at both sides of the line defect. An analytical expression about the transmission probability can be then obtained. To write out the results of both valleys together, the transmission probability takes a form as

$$T_{K(K')} = |t_{K(K')}|^2 = \frac{\mathcal{F}^2 \cos^2\theta}{1 + \mathcal{F}^2 \pm 2\mathcal{F}\sin\theta}, \tag{23}$$

where $+$ and $-$ correspond to $\mathbf{K}$ and $\mathbf{K}'$ valleys respectively. The incident angle θ is just the angle of the electronic wavevector $\mathbf{k} = (k_x, k_y)$ with respect to x axis. Surprisingly, such an exact result is the same as the expression of the transmission probability estimated in zero-energy limit in Ref. [17]. This indicates that the energy independent transmission probability through a line defect is an intrinsic electronic property of graphene if only the electron energy is restricted in the linear dispersion region.

IV. SUMMARY

In this work, we study the applicability of the Dirac-equation approach to describe the electronic properties of graphene when a line defect appears. With the help of the TB model, we have established an appropriate connection condition for the spinor wavefunction across the line defect. As a result, the massless 2D Dirac equation is still a valid theoretical model to describe low-energy electronic characteristics of graphene in the presence of a line defect. To check the validity of the wavefunction connection condition, we have taken two kinds of line defect embedded graphene structures as examples to work out the low-energy electronic states from Dirac equation. For the LD-ZGNR structures, we find that the Dirac equation subject to the wavefunction connection condition across the line defect and the boundary condition at the ribbon edges provides analytical results about the low-energy subband structure and the corresponding eigen wavefunction. These results agree well with the numerical results from the TB model even when the smaller characteristic width of the LD-ZGNR is as small as 10nm. For an LD-BG, we have derived an exact expression about the electronic transmission probability through the line defect, which demonstrates the valley polarization and the energy independence of the electronic transmission probability estimated in zero-energy limit in a previous work.[17] More interestingly, our analytical result indicates that in such a 2D graphene structure a quasi 1D electronic state exists along the extended line defect. And the electronic group velocity in this quasi 1D electronic state can be readily modulated by applying a strain field along the line defect. As a result, the line defect can be viewed as a 1D quantum wire to carry the current in a bulk graphene sample.

A remarkable advantage of the Dirac-equation approach supplemented by the wavefunction connection condition over the TB model and ab *initio* calculation approach is that analytical solutions about the electronic states are accessible in many cases. Thus the resultant electronic properties can be understood or anticipated in an intuitive way. With the wavefunction connection condition we have established in this work, many electronic characteristics of graphene in the presence of a line defect can be further studied by Dirac-equation approach, for example, the subband structure of a line defect superlattice of graphene, the magnetic minibands and magneto-transport properties of some line defect embedded graphene structures when a perpendicular magnetic field is applied. In addition, our theoretical method can be generalized to obtain the spinor wavefunction connection conditions when other kinds of line defects emerge in graphene.

V. ACKNOWLEDGEMENTS

[*] Author to whom correspondence should be addressed. Email address: `zys@jlu.edu.cn`

[1] T. R. Albrecht, H. A. Mizes, J. Nogami, S-i. Park and C. F. Quate, Appl. Phys. Lett. **52**, 362 (1988).

[2] C. R. Clemmer and T. P. Beebe, Science **251**, 640 (1991).

[3] W. M. Heckl and G. Binnig, Ultramicroscopy **42**, 1073 (1992).

[4] J. Červenka and C. F. J. Flipse, Phys. Rev. B **79**, 195429 (2009).

[5] J. Červenka, M. I. Katsnelson and C. F. J. Flipse, Nature Phys. **5**, 840 (2009).

[6] J. Coraux *et al.*, New J. Phys. **11**, 023006 (2009).

[7] D. L. Miller *et al.*, Science **324**, 924 (2009).

[8] E. Loginova, S. Nie, K. Thurmer, N. C. Bartelt and K. F. McCarty, Phys. Rev. B **80**, 085430 (2009).

[9] H. J. Park, J. Meyer, S. Roth and V. Skákalová, Carbon **48**, 1088 (2010).

[10] J. Lahiri, Y. Lin, P. Bozkurt, I. I. Oleynik, and M. Batzill, Nature Nanotech. **5**, 326 (2010).

[11] A. P. Sutton and R. W. Balluffi, *Interfaces in Crystalline Materials*, Clarendon Press (1995).

[12] O.V. Yazyev and S. G. Louie, Nature Mater. **9**, 806 (2010).

[13] D. J. Appelhans, L. D. Carr and M. T. Lusk, New J. Phys., **12**, 125006 (2010).

[14] X. Li, C. W. Magnuson, A. Venugopal, R. M. Tromp, J. B. Hannon, E. M. Vogel, L. Colombo and R. S. Ruoff, J. Am. Chem. Soc. **133**, 2816 (2011).

[15] Q. Yu, A. L. Jauregui, W. Wu, R. Colby, J. Tian, Z. Su, H. Cao, Z. Liu, D. Pandey, D. Wei, T. F. Chung, P. Peng, N. P. Guisinger, E. A. Stach, J. Bao, S. Pei and Y. Chen, Nature Mater. **10**, 443 (2011).

[16] F. Banhart, J. Kotakoski, and A. V. Krasheninnikov, ACS Nano **5**, 26 (2011).

[17] D. Gunlycke and C. T. White, Phys. Rev. Lett. **106**, 136806 (2011).

[18] D. Gunlycke and C. T. White, J. Vac. Sci. Technol. B **30**, 03D112 (2012).

[19] D. A. Bahamon, A. L. C. Pereira, and P. A. Schulz, Phys. Rev. B **83**, 155436 (2011).

[20] X. Lin and J. Ni, Phys. Rev. B **84**, 075461 (2011).

[21] J. C. Slonczewski and P. R. Weiss, Phys. Rev. **109**, 272 (1958).

[22] G. W. Semenoff, Phys. Rev. Lett. **53**, 2449 (1984).

[23] F. D. M. Haldane, Phys. Rev. Lett. **61**, 2015 (1988).

[24] Y. Zheng and T. Ando, Phys. Rev. B **65**, 245420 (2002).

[25] T. Ando, J. Phys. Soc. Jpn. **74**, 777 (2005).

[26] A. H. C. Neto, F. Guinea, N. M. R. Peres, K. S. Novoselov and A. K. Geim, Rev. Mod. Phys. **81**, 109 (2009).

[27] M. I. Katsnelson, K. S. Novoselov and A. K. Geim, Nature Phys. **2**, 620 (2006).

[28] Y. Zhang, Y. W. Tan, H. L. Stormer and P. Kim, Nature **438**, 201 (2005).

[29] L. Brey and H. A. Fertig, Phys. Rev. B **73**, 235411 (2006).

[30] J. A. M. van Ostaay, A. R. Akhmerov, C. W. J. Beenakker, and M. Wimmer, Phys. Rev. B **84**, 195434 (2011).

[31] A. R. Akhmerov and C. W. J. Beenakker, Phys. Rev. B **77**, 085423 (2008).

[32] D. P. DiVincenzo and E. J. Mele, Phys. Rev. B **29**, 1685 (1984).

[33] L. Jiang, X. Lv, and Y. Zheng, Phys. Lett. A **376**, 136 (2011).

FIG. 1: (Color online) Lattice structure of a zigzag-edged graphene nanoribbon embedded with an extended line defect along the longitudinal direction (y direction). The shadow region denotes a unit cell of such a structure. $2a$ (a is the lattice constant of a pristine graphene) is the primitive translational vector along y direction when the extended line defect is present. The light (grey) solid circles are the atoms at the line defect. The hollow circles and heavy solid circles denote the atoms in A and B sublattices respectively. The integer n denotes the layer number and j specifies an individual atom in a given layer. The ribbon width is $W = L_1 + L_2$ with L_1 and L_2 are two characteristic widths to measure the transverse sizes of the ribbon on the opposite side of the line defect. When $L_1 = L_2 \to \infty$, this structure becomes a bulk graphene with the line defect at $x = 0$.

FIG. 2: (Color online) Low-energy subbands of the LD-ZGNR in $\mathbf{K}$ valley calculated by Dirac-equation and TB approaches. The characteristic width L_1 is fixed at $L_1 = 75\sqrt{3}a$. (a) The case of $L_2 = 25\sqrt{3}a$. (b) Enlarged view of (a) in the wavevector range $-0.3/2a \leq k_y \leq 0.4/2a$. (c) The case of $L_2 = 5\sqrt{3}a$. (d) Enlarged view of (c) in the wavevector range $-0.3/2a \leq k_y \leq 0.13/2a$. The three points labeled by $(1, 2, 3)$ specify the eigen states selected to show their electronic probability distributions on lattice points in a unit cell in Fig. 3.

FIG. 3: (Color online) The electronic probability distributions of the selected three eigen states marked in Figs. 2(c) and (d) with the characteristic widths of the LD-ZGNR being $L_1 = 75\sqrt{3}a$ and $L_2 = 5\sqrt{3}a$. The results depicted by square and triangle symbols are from the TB calculations, while the solid and dashed lines show the results from the Dirac-equation approach. (a) The case of point 1 in Fig. 2(d). (b) The case of point 2 in Fig. 2(d). (c) The case of point 3 in Fig. 2(c).

FIG. 4: (Color online) Comparison between TB and Dirac-equation calculations for the dispersion relation of the quasi 1D state of an LD-BG at $\mathbf{K}$ valley. The low-energy bulk band (gray) shows the Dirac-cone-like structure. The TB results are calculated by means of an LD-ZGNR of $L = 500\sqrt{3}a$ subject to a periodic boundary condition.
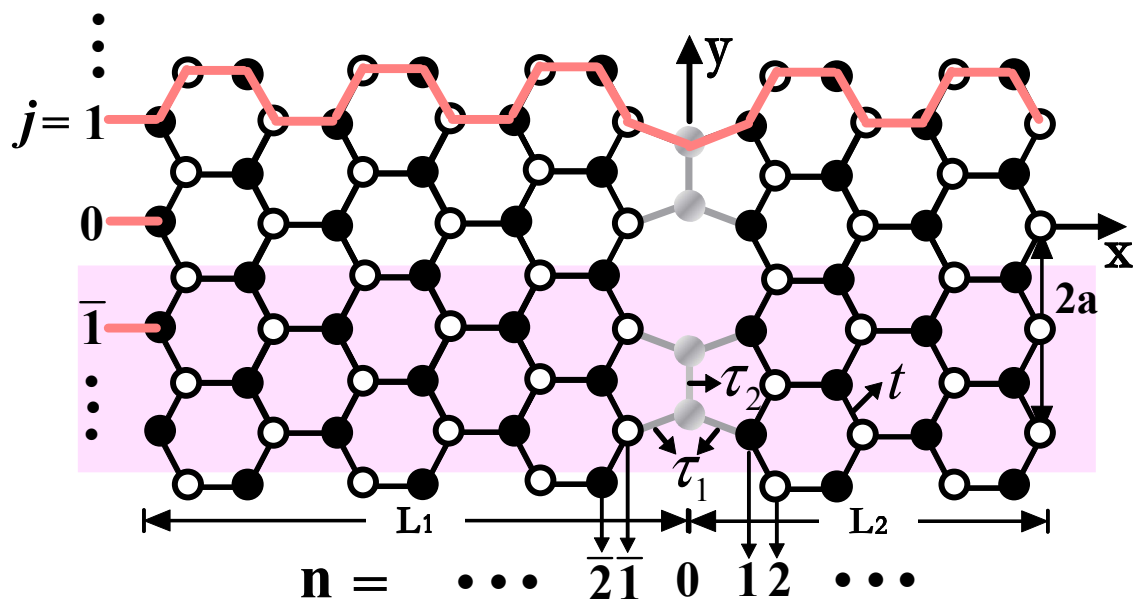
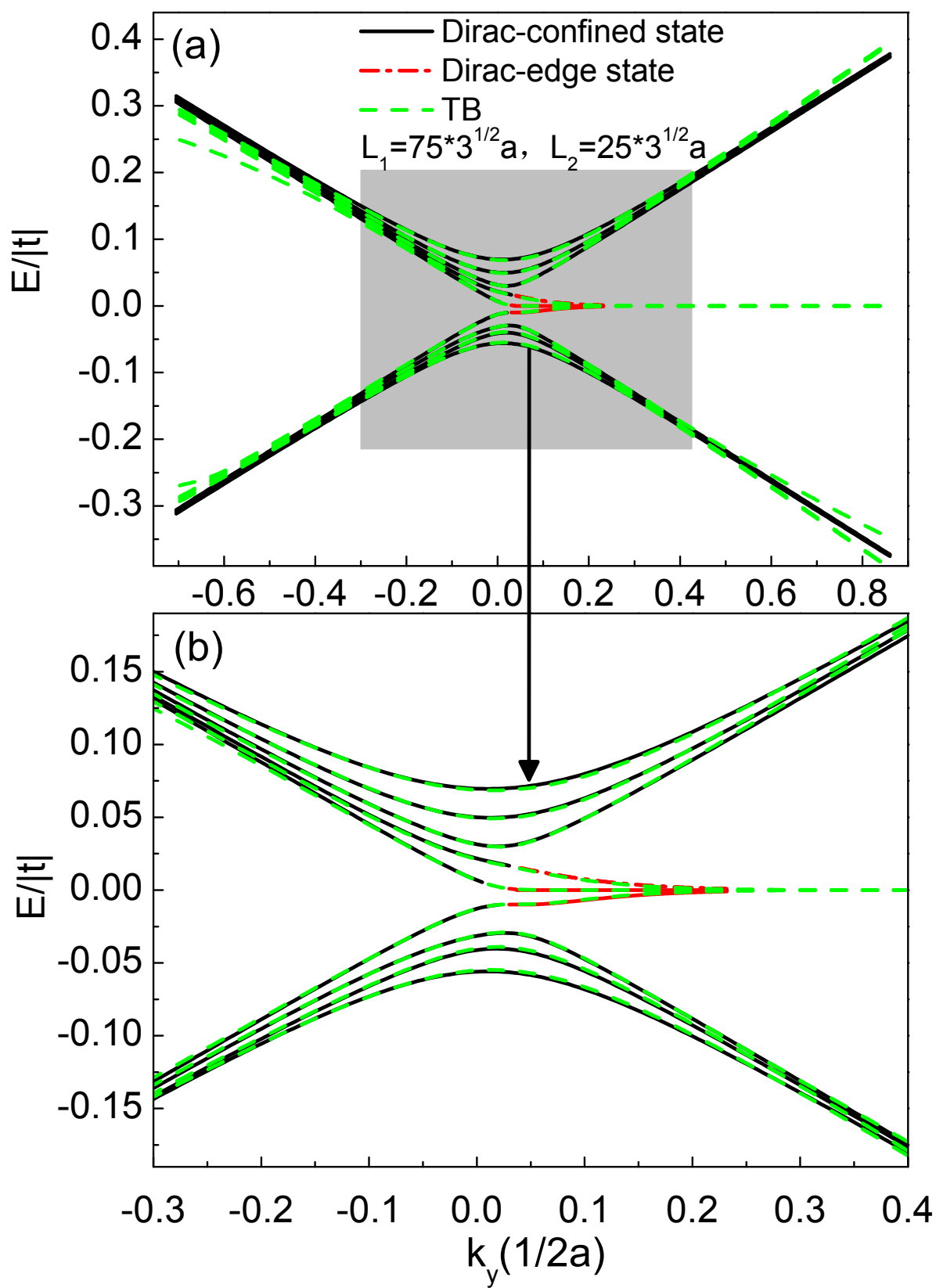Figure 1   BU12010   14Sep2012

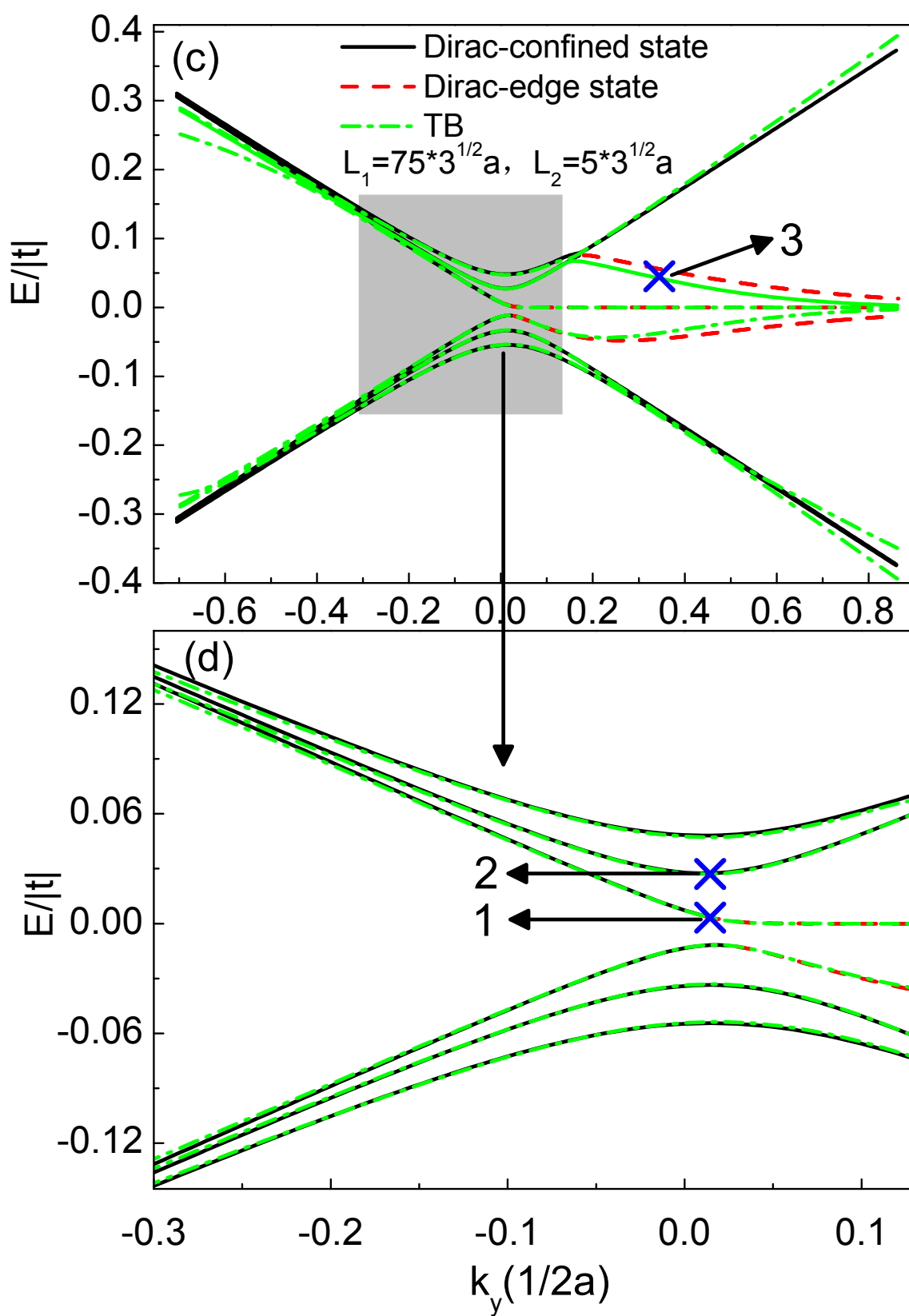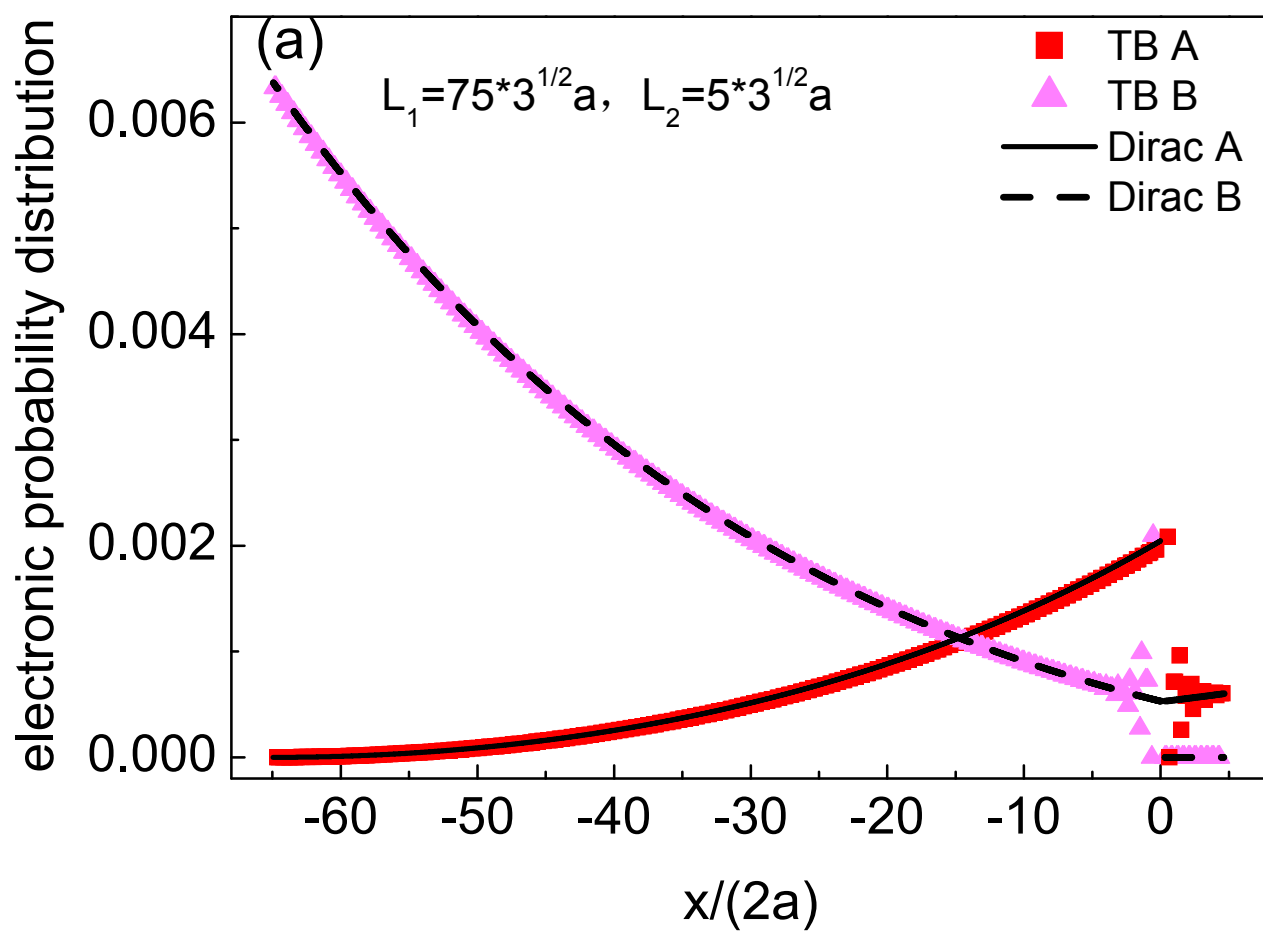Figure 2ab   BU12010   14Sep2012
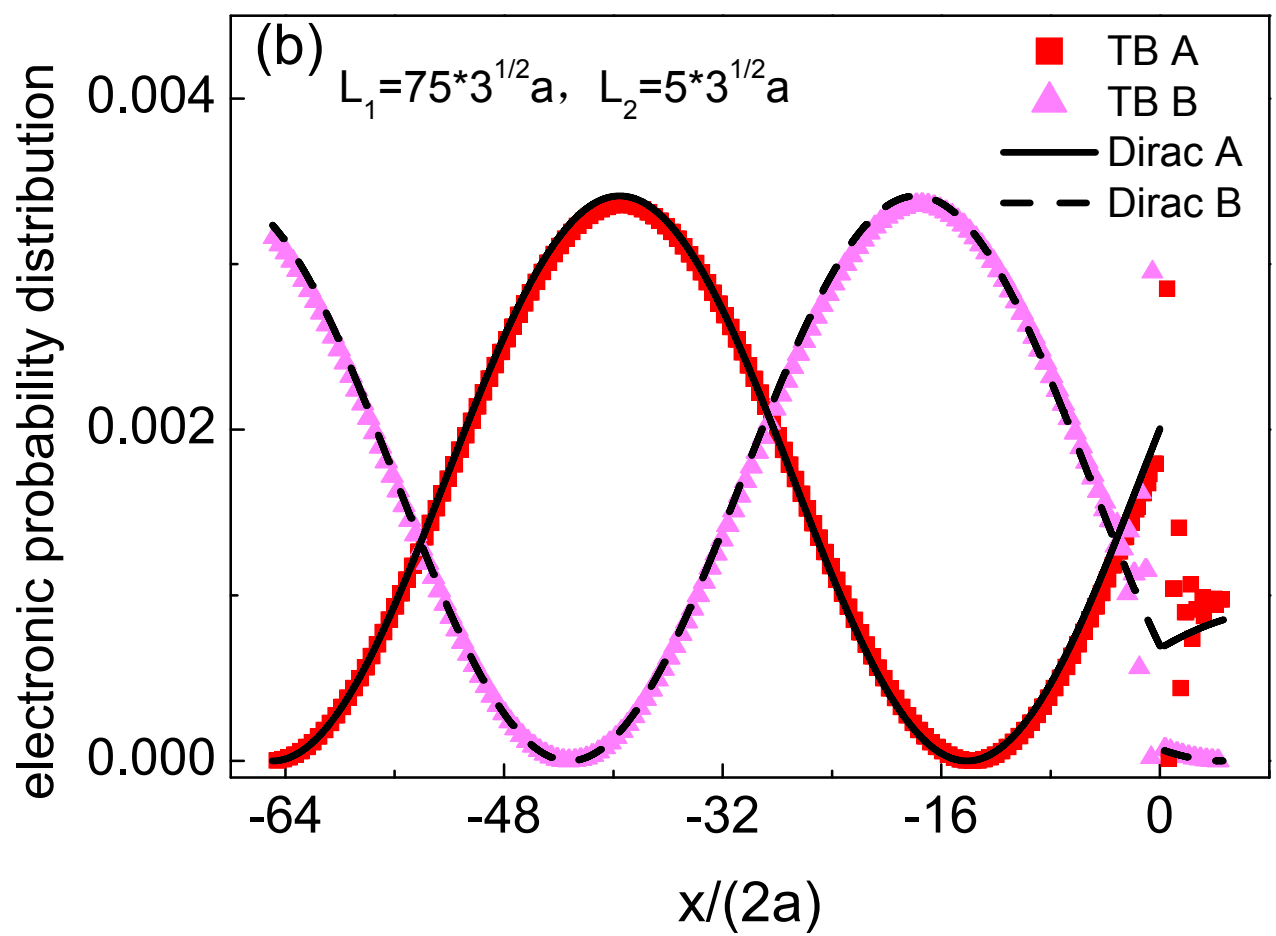
Figure 2cd   BU12010   14Sep2012

(a)

$L_1 = 75 \cdot 3^{1/2} a$, $L_2 = 5 \cdot 3^{1/2} a$

electronic probability distribution

x/(2a)

- TB A
- TB B
- Dirac A
- Dirac B

Figure 3a   BU12010   14Sep2012

(b)

$L_1 = 75*3^{1/2}a$, $L_2 = 5*3^{1/2}a$

electronic probability distribution

x/(2a)

- TB A
- TB B
- Dirac A
- Dirac B

0.004
0.002
0.000

-64   -48   -32   -16   0
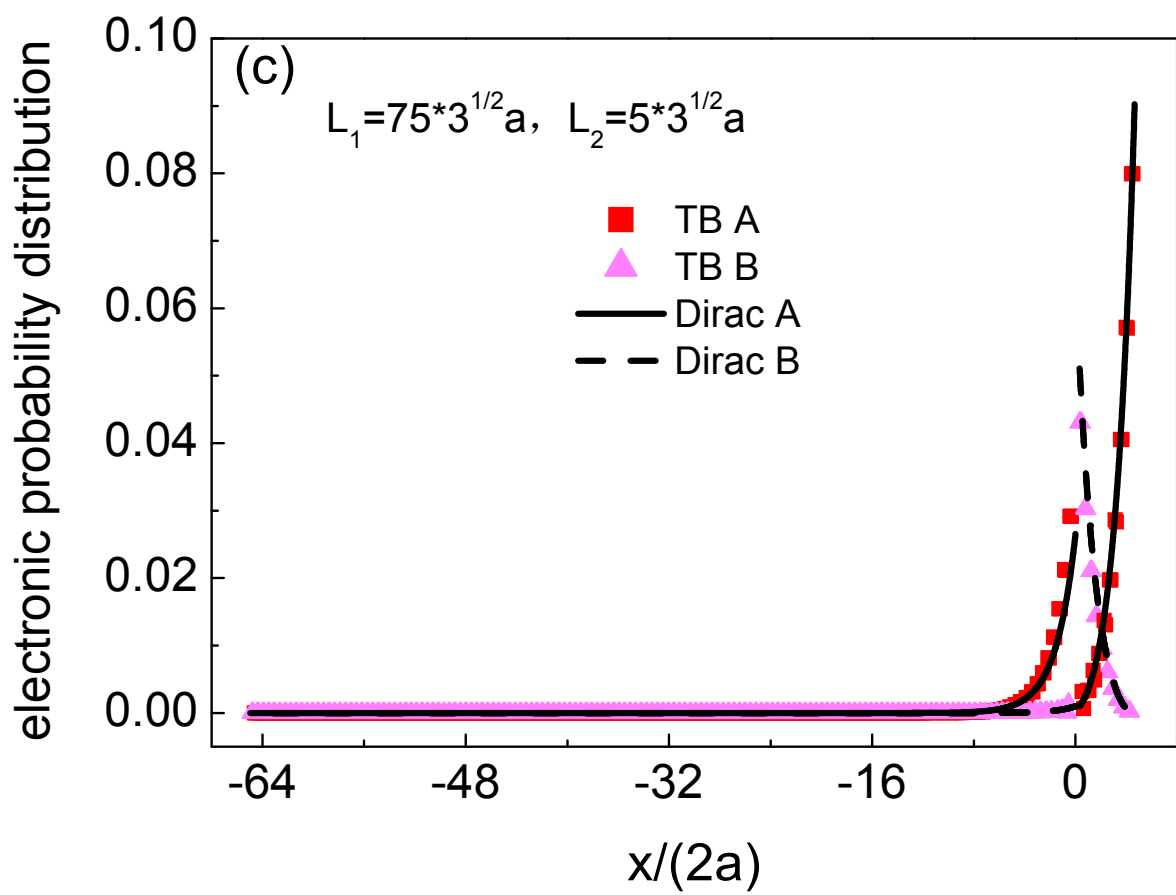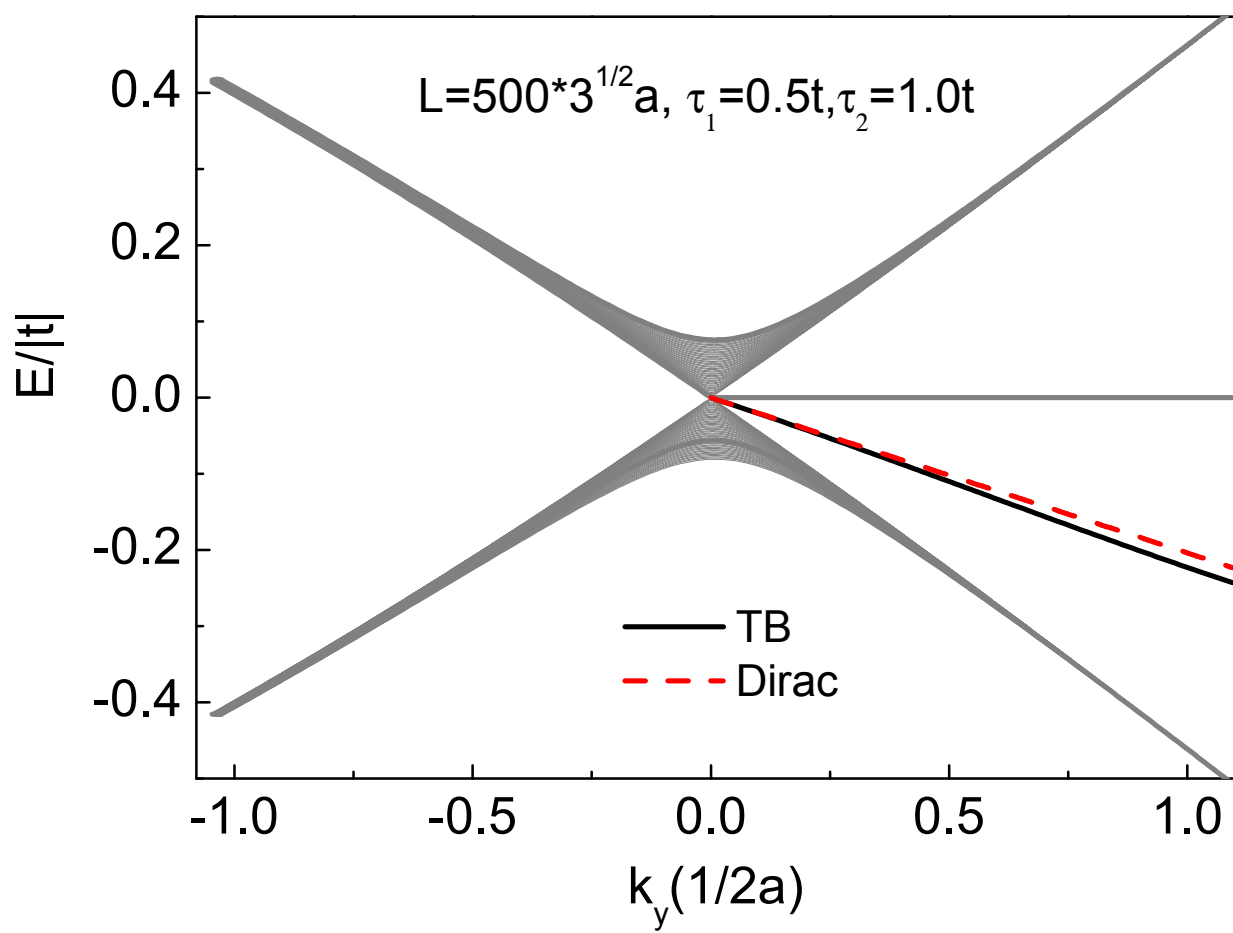
Figure 3b   BU12010   14Sep2012

Figure 3c   BU12010   14Sep2012

Figure 4   BU12010   14Sep2012